A widely tunable few-electron droplet



2007 J. Phys.: Condens. Matter 19 236202

(http://iopscience.iop.org/0953-8984/19/23/236202)

IOP PUBLISHING JOURNAL OF PHYSICS: CONDENSED MATTER

J. Phys.: Condens. Matter **19** (2007) 236202 (10pp) doi:10.1088/0953-8984/19/23/236202

# A widely tunable few-electron droplet

**A K Hüttel[1,3], K Eberl[2,4] and S Ludwig[1]**

[1] Center for NanoScience and Department für Physik, Ludwig-Maximilians-Universität, Geschwister-Scholl-Platz 1, 80539 München, Germany
[2] Max-Planck-Institut für Festkörperforschung, Heisenbergstraße 1, 70569 Stuttgart, Germany

E-mail: A.K.Huettel@tudelft.nl

Received 31 January 2007, in final form 9 April 2007
Published 8 May 2007
Online at stacks.iop.org/JPhysCM/19/236202

**Abstract**

Quasi-static transport measurements are employed to characterize a few-electron quantum dot electrostatically defined in a GaAs/AlGaAs heterostructure. The gate geometry allows observations on one and the same electron droplet within a wide range of coupling strengths to the leads. The weak coupling regime is described by discrete quantum states. At strong interaction with the leads, Kondo phenomena are observed as a function of a magnetic field. By varying the gate voltages the electron droplet can, in addition, be distorted into a double quantum dot with a strong interdot tunnel coupling while keeping track of the number of trapped electrons.

(Figures in this article are in colour only in the electronic version)

## 1. Introduction

Extensive experimental work has recently been aimed towards electrostatically defining and controlling semiconductor quantum dots [1–5]. These efforts are impelled by proposals for using localized electron spin [6] or charge states [7], respectively, as qubits, the elementary registers of the hypothetical quantum computer. The complete control of the quantum dot charge down to the limit of only one trapped conduction band electron was demonstrated by monitoring single electron tunnelling (SET) current through the device as well as by a nearby charge detector [2, 8, 9].

In this paper, we present data on an electron droplet in which the charge can be controlled all the way to the limit of one electron. The quantum dot is defined electrostatically by using split gates on top of an epitaxially grown AlGaAs/GaAs heterostructure. We observe a wide tunability of the electronic transport properties of our device. Recent work focused either on the case of weak coupling between a quantum dot and its leads [2], or on the Kondo regime of strong coupling to the leads [9]. Here, we explore a structure that can be fully tuned between

[3] Present address: Molecular Electronics and Devices, Kavli Institute of Nanoscience, Delft University of Technology, PO Box 5046, 2600 GA Delft, The Netherlands.
[4] Present address: Lumics GmbH, Carl-Scheele-Strasse 16, 12489 Berlin, Germany.

  

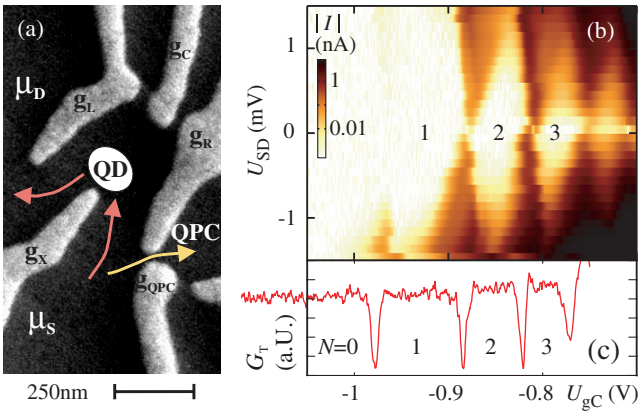


**Figure 1.** (a) SEM micrograph of the gate electrodes used to electrostatically define a quantum dot (marked as QD) and a quantum point contact (marked as QPC). (b) Typical measurement of the absolute value of the SET current $I$ through the quantum dot as a function of the centre gate voltage $U_{gC}$ and the bias voltage $U_{SD}$. (c) Differential transconductance $G_T(U_{gC})$ of the QPC measured at identical parameters as in (b) but for $U_{SD} = 0$. The numerals $N = 0, 1, 2, 3$ in (b) and (c) depict the actual number of conduction band electrons trapped in the quantum dot.

these limits. In addition, we demonstrate how the shape of the quantum dot confinement potential can be distorted within the given gate geometry [10] all the way into a double well potential describing a double quantum dot [11–13]. The charge of the electron droplet can be monitored during the deformation process.

The heterostructure used for the measurements embeds a two-dimensional electron system (2DES) 120 nm below the crystal surface. The electron sheet density and mobility in the 2DES at the temperature of $T = 4.2$ K are $n_s \simeq 1.8 \times 10^{15}\,\mathrm{m}^{-2}$ and $\mu \simeq 75\,\mathrm{m}^2\,\mathrm{V}^{-1}\,\mathrm{s}^{-1}$, respectively. We estimate the 2DES temperature to be of the order $T_{2DES} \sim 100$ mK.

Our gate electrode geometry for defining a quantum dot, shown in the scanning electron microscope (SEM) micrograph of figure 1(a), is designed following a geometry introduced by Ciorga *et al* [2]. Because of the triangular shape of the confinement potential, an increasingly negative voltage on the plunger gate $g_C$ depletes the quantum dot and simultaneously shifts the potential minimum towards the tunnel barriers defined by gates $g_X$ and $g_L$, or $g_X$ and $g_R$, respectively. This way, the tunnel barriers between the leads and the electron droplet can be kept transparent enough to allow the detection of SET current through the quantum dot even for an arbitrarily small number of trapped conduction band electrons [2].

Figure 1(b) shows a typical colour scale plot of the measured quantum dot SET current $|I|$ as a function of the gate voltage $U_{gC}$ and the source drain voltage $U_{SD}$. Within the diamond-shaped light regions in figure 1(b) SET is hindered by Coulomb blockade, and the charge of the quantum dot is constant. The gates marked $g_R$ and $g_{QPC}$ in figure 1(a) are used to define a quantum point contact (QPC). As demonstrated in [8] and [9], a nearby QPC can provide a non-invasive way to detect the charge of a quantum dot electron by electron. The result of such a measurement is shown in figure 1(c), where the transconductance $G_T = \mathrm{d}I_{QPC}/\mathrm{d}U_{gC}$ obtained using a lock-in amplifier is plotted for $U_{SD} \simeq 0$, along the corresponding horizontal trace in figure 1(b). Note that figures 1(b) and (c) have identical $x$ axes. The advantage of using a QPC charge detector is that its sensitivity is almost independent of the quantum dot charge state. In contrast, the current through the quantum dot decreases as it is discharged electron by electron, because of an increase of the tunnel barriers between the quantum dot and the leads. This can be clearly seen by a comparison of the magnitude of the current oscillations in figure 1(b) with

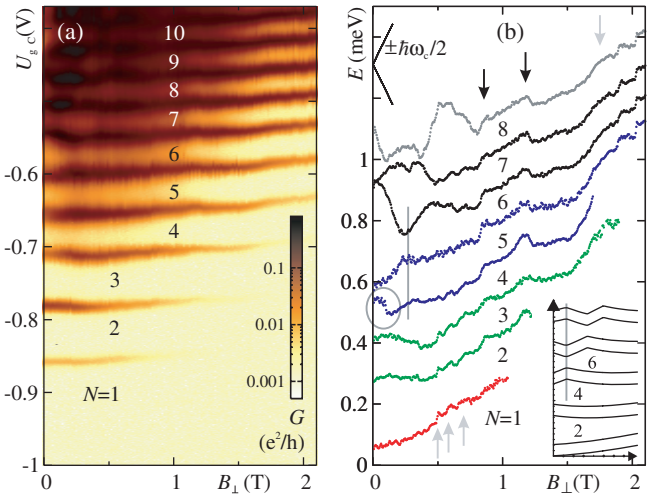


**Figure 2.** (a) The dependence of the differential conductance $G$ of the quantum dot on a magnetic field $B_\perp$ perpendicular to the 2DES and the voltage on gate $g_C$. All other gate voltages are kept fixed (see main text). (b) The $B_\perp$ dependence of a relative energy corresponding to the local maxima of $G$. The traces are numerically obtained from the measurement shown in (a) after a conversion of the gate voltage to energy and subtraction of an arbitrary but $B_\perp$-independent energy, respectively. Black arrows mark common features of all traces. The grey vertical line indicates the first ground state transition of the quantum dot for $N \gtrsim 4$. Inset: qualitative prediction for the traces, using a Fock–Darwin potential and the constant interaction model.

the transconductance minima in figure 1(c)[5]. The QPC transconductance measurement plotted in figure 1(c) shows no pronounced local minima corresponding to changes of the quantum dot charge for $U_{gC} < -1$ V. This indicates that the quantum dot is here entirely uncharged. This observation has been confirmed by further careful tests as for example variation of the tunnel barriers or variation of the QPC lock-in frequency and QPC bias. The inferred number of conduction band electrons $N = 0, 1, \ldots$ trapped in the quantum dot is indicated in the Coulomb blockade regions in figures 1(b) and (c)[6].

In the following we demonstrate the flexibility provided by the use of voltage tunable top-gates for a lateral confinement of a 2DES. We first focus on the regime of a few-electron quantum dot weakly coupled to its leads, where the shell structure of an artificial two-dimensional atom in the circularly symmetric case is described by the Fock–Darwin states [14, 15]. Secondly, we present measurements with the quantum dot strongly coupled to its leads. Here we observe Kondo features. Finally, we explore the deformation of the few-electron droplet into a serial double quantum dot by means of changing gate voltages. The transport spectrum of this artificial molecule has been described in previous publications for the low electron number limit ($0 \leqslant N \leqslant 2$) [11–13, 16].

## 2. Weak coupling to the leads

The regime of a few-electron quantum dot weakly coupled to its leads is reached for gate voltages of $U_{gL} = -0.52$ V, $U_{gR} = -0.565$ V, and $U_{gX} = -0.3$ V. The observed Coulomb blockade oscillations are shown in figure 2(a), where the differential conductance

[5] An apparent double peak structure in figure 1(b) around $U_{SD} \sim 0$ can be explained by noise rectification effects.
[6] The SET current shown in figure 1(b) between $N = 0$ and 1 cannot be resolved for $U_{SD} \sim 0$. We ascribe this to an asymmetric coupling of the quantum dot to the leads.

$G \equiv \mathrm{d}I/\mathrm{d}U_{\mathrm{SD}}$ of the quantum dot is plotted in a logarithmic (colour) scale as a function of centre gate voltage $U_{\mathrm{gC}}$ and magnetic field perpendicular to the 2DES $B_\perp$. The absolute number $N$ of trapped electrons within the Coulomb blockade regions, derived by means of the QPC charge detection, is indicated by numerals.

The characteristic $B_\perp$ dependence of the local maxima of differential conductance in figure 2(a), marking the Coulomb oscillations of SET, has also been observed via capacitance spectroscopy of lateral quantum dots [17] and via transport spectroscopy of vertically etched quantum dots [18].

The addition energy of a quantum dot for each electron number $N$ can be derived from the vertical distance (in $U_{\mathrm{gC}}$) between the local SET maxima, by converting the gate voltage scale $U_{\mathrm{gC}}$ into a local potential energy. The conversion factor for the present quantum dot has been obtained from nonlinear transport measurements; a constant conversion factor is used as a first-order approximation [1]. Accordingly, in figure 2(b) the $B_\perp$ dependence of the differential conductance maxima positions is plotted after conversion to energy scale. The traces are obtained by numerically tracking the local SET maxima in figure 2(a). An arbitrary but $B_\perp$-independent energy is subtracted from each trace, such that all traces are equidistant at $B_\perp = 1$ T—i.e. at a magnetic field high enough such that orbital effects are no longer relevant to the $B_\perp$ dependence of the addition energy. For a direct comparison the inset of figure 2(b) displays the $B_\perp$ dependence expected within the so-called constant interaction model [1], that approximates many-particle effects with a classical capacitance term, for the so-called Fock–Darwin states. These are solutions of the single-particle Schrödinger equation of a 'two-dimensional atom'. In detail the vector potential of $B_\perp$ and the Fock–Darwin potential $V = m^*\omega_0^2 r^2/2$ are considered. The latter describes a two-dimensional harmonic oscillator with characteristic frequency $\omega_0$ and effective electron mass $m^*$, at the distance $r$ from its potential minimum [14, 15]. The harmonic approximation is justified for a few-electron quantum dot with a relatively smooth electrostatic confinement as usually provided by remote gate electrodes.

Although not necessarily expected for lateral quantum dots, where the tunnel barriers to the 2DES leads automatically induce symmetry breaking, for electron numbers $1 \leqslant N \leqslant 7$ the measured $B_\perp$ dependence (figure 2(b)) resembles these model expectations (inset). The observed and predicted pairing of SET differential conductance maxima corresponds to an alternating filling of two-fold spin-degenerate levels [18–20].

A local maximum of addition energy is visible at $N = 6$, which would correspond to a filled shell in a circular symmetric potential [18]. For $4 \leqslant N \leqslant 7$ the first orbital ground state transition is visible as cusps at $0.25\ \mathrm{T} \lesssim B_\perp \lesssim 0.3\ \mathrm{T}$. The cusps are marked by a vertical grey line in figure 2(b) and its inset, respectively. The magnetic field at which this transition happens allows us to estimate the characteristic energy scale of the confinement potential [21] $\hbar\omega_0 = \sqrt{2}\,\hbar\omega_{\mathrm{c}}(B_\perp) \sim 680\,\mu\mathrm{eV}$. The expected maximum slopes of the $E(B_\perp)$ traces are given by the orbital energy shift and are expected to be of the order of $\mathrm{d}E/\mathrm{d}B_\perp = \pm\hbar\omega_{\mathrm{c}}/2B$, where $\omega_{\mathrm{c}} = eB_\perp/m^*$ is the cyclotron frequency in GaAs. These expected maximum slopes are indicated in the upper-left corner of figure 2(b) and agree well with our observations.

For the $4 \leqslant N \leqslant 5$ transition and at a small magnetic field $B_\perp \lesssim 0.2$ T our data exhibit a pronounced cusp marking a slope reversal, as indicated by the grey ellipsoid in figure 2(b). This deviation from the prediction of the constant interaction model seems similar to the consequences of Hund's rules as observed in quantum dots with high circular symmetry [18]. Along this model the electronic exchange energy would be estimated as $J \sim 90\,\mu\mathrm{eV}$ for the involved states. However, an according deviation from the constant interaction model for the $3 \leqslant N \leqslant 4$ transition [18] predicted by Hund's rules is not observed here. Therefore, and since a clear rotational symmetry is never present in lateral quantum dots, a definite

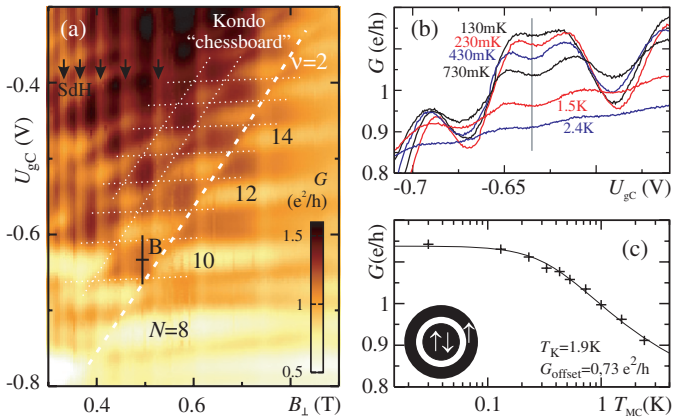


**Figure 3.** (a) Differential conductance $G$ at strong coupling to the leads as a function of perpendicular magnetic field $B_\perp$ and gate voltage $U_{gC}$. A distinct chessboard-like pattern of enhanced conductance is observed (see dotted lines). Black arrows mark Shubnikov–de Haas conductance minima of the 2DES in the leads. (b) Conductance traces $G(U_{gC})$ at constant $B_\perp = 495$ mT for different cryostat temperatures. The traces are measured along the vertical line marked with 'B' in (a). (c) Cryostat temperature dependence of the conductance $G$ at $B_\perp = 495$ mT and $U_{gC} = -0.635$ V (vertical grey line in (b)). The solid line is a model curve for a Kondo temperature of $T_K = 1.9$ K (see text for details).

identification of this ground state transition observed in our measurements is not possible. For $N \geqslant 7$ the $E(B_\perp)$ traces no longer resemble the Fock–Darwin state predictions. We attribute this to modifications of the transport spectrum caused by electron–electron interactions. In addition, the measurements plotted in figure 2(a) indicate strong co-tunnelling currents within the Coulomb blockade regions for $N \gtrsim 7$. This can be seen by the growing conductance in the Coulomb blockade regions as the electron number is increased.

At the magnetic fields of $B_\perp \simeq 0.88$ T and $B_\perp \simeq 1.17$ T, all traces exhibit a common shift, as marked by black arrows in figure 2(b). This may be explained by an abrupt change of the chemical potential in the leads, since at these magnetic fields the 2DES in the leads reaches even integer filling factors of $\nu_{2DES} = 8$ and $\nu_{2DES} = 6$, respectively[7]. The integer filling factors of the 2DES have been identified in the Coulomb blockade measurements up to $\nu_{2DES} = 1$ at $B \simeq 7.1$ T, where, as in previous publications [2, 22], also a shift at odd $\nu_{2DES}$ is observed (data not shown)[8].

## 3. Strong coupling to the leads

By increasing the voltages on the side gates $U_{gL}$ and $U_{gR}$ the quantum dot in the few-electron limit is tuned into a regime of strong coupling to the leads. During this process the position of the SET differential conductance maxima is tracked so that the quantum dot charge state remains well known. At strong coupling we observe enhanced differential conductance in Coulomb blockade regions due to the Kondo effect [23–25].

Figure 3(a) shows part of the transport spectrum of the quantum dot as a function of $B_\perp$ and $U_{gC}$ at $U_{gL} = -0.508$ V, $U_{gR} = -0.495$ V, and $U_{gX} = -0.3$ V. Compared to the weak

[7] A step-like feature in the data at $B_\perp \simeq 1.75$ T can be identified with the filling factor $\nu_{2DES} = 4$ (grey arrow in figure 2(b)); however, here the observation is far less clear than at $\nu_{2DES} = 6$ and $\nu_{2DES} = 8$. At higher filling factors $\nu_{2DES} = 10, 12, \ldots$ (also grey arrows) the effect diminishes and is partially shadowed by the orbital transitions.

[8] The magnetic field has in all measurements been stepped towards higher field values. These results are thus consistent with a shift caused by long-living eddy currents in the 2DES of the leads, as discussed in [22].

coupling case displayed in figure 2 the SET differential conductance maxima (almost horizontal lines) are broader in figure 3. This broadening can be explained by a much stronger coupling to the leads. In addition, a background differential conductance increases monotonically towards more positive gate voltage $U_{\mathrm{gC}}$. This background is independent of the Coulomb blockade oscillations. The quantum dot is here near the mixed valence regime where charge quantization within the confinement potential is lost. Thus, the conductance background is explained by direct scattering of electrons across the quantum dot. Vertical lines of decreased differential conductance, marked in figure 3(a) with black arrows, indicate minima in the density of states at the Fermi energy of the lead 2DES caused by Shubnikov–de Haas oscillations.

Between the maxima of SET differential conductance Coulomb blockade is expected. Instead we observe a distinct chessboard-like pattern of areas of enhanced or suppressed differential conductance, in the region highlighted by the white dashed or dotted lines in figure 3(a). This feature is independent of the Shubnikov–de Haas oscillations (vertical lines). Similar phenomena have already been observed in many-electron quantum dots and have been identified as a $B_\perp$-dependent Kondo effect [26]. For the many-electron regime, they have been modelled such that the magnetic field perpendicular to the 2DES leads to the formation of Landau-like core and ring states in the quantum dot, as sketched in figure 3(c) [27, 28]. The electrons occupying the lowermost Landau level effectively form an outer ring and dominate the coupling of the quantum dot to its leads, whereas the higher Landau-like levels form a nearly isolated electron state in the core of the quantum dot [27, 29, 30][9]. On one hand, with increasing magnetic field one electron after the other moves from the core into the outer ring, and hence the total spin of the strongly coupled outer ring can oscillate between $S = 0$ and $1/2$. Only for a finite spin does the Kondo effect cause an enhanced differential conductance. On the other hand a change in $U_{\mathrm{gC}}$ eventually results in a change of the total number and total spin of the conduction band electrons trapped in the quantum dot.

In addition, charge redistributions between the levels of the quantum dot may influence the SET maxima positions [9, 27, 30]. The combination of these effects explains the observed chessboard-like pattern of enhanced and suppressed differential conductance through the quantum dot. For a higher magnetic field where the filling factor falls below $\nu = 2$ inside the electron droplet a separation in outer ring and core state cannot exist any longer. The chessboard-like pattern disappears and the Kondo effect is expected to depend monotonically on $B_\perp$. Indeed, for $B_\perp$ larger than a field marked by the dashed white line in figure 3(a) the Kondo current stops oscillating as a function of $B_\perp$. From this we conclude that the dashed white line in figure 3(a) identifies the $\nu = 2$ transition inside the quantum dot.

Figure 3(b) displays exemplary traces $G(U_{\mathrm{gC}})$ of the differential conductance as a function of the gate voltage $U_{\mathrm{gC}}$ at a fixed magnetic field $B_\perp = 495$ mT for different cryostat temperatures. These traces are taken along the black vertical line in figure 3(a) marked by 'B'. The vertical line in figure 3(b) marks the expected position of a minimum of the differential conductance due to Coulomb blockade, as indeed observed for the traces recorded at high temperature. At low temperature, instead of a minimum an enhanced differential conductance is measured due to the Kondo effect. Note that the two minima of the differential conductance adjacent to the Kondo feature in figure 3(b) show the usual temperature behaviour, indicating that here the Kondo effect is absent (in accordance with the chessboard-like pattern in figure 3(a)). Figure 3(c) displays the differential conductance at the centre of the Coulomb blockade region marked by the vertical line in figure 3(b), as a function of the cryostat temperature. The solid line is a model curve given by

[9] As has been shown by the authors of [9], a comparable model based on single-particle Fock–Darwin states still describes measurements successfully down to the range of low electron numbers $7 \leqslant N \leqslant 9$. In close analogy, reference [9] describes the transport spectrum in terms of 'localized' and 'extended' electron states.

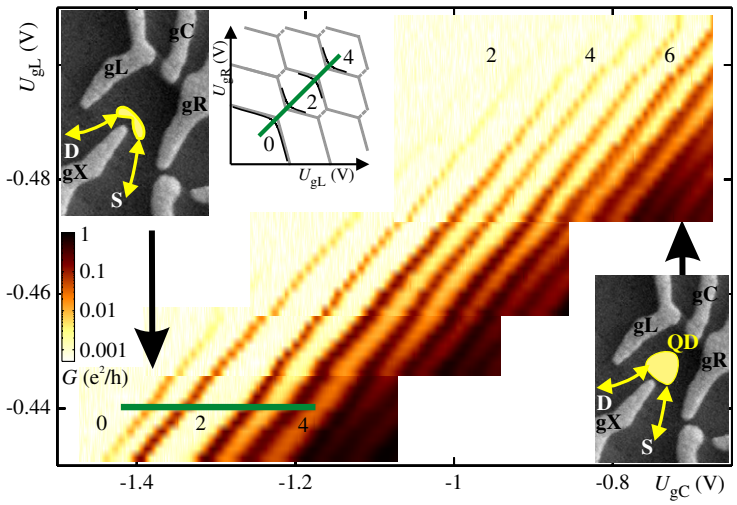


**Figure 4.** Differential conductance of the electron droplet as a function of $U_{gC}$ ($x$ axis) and the simultaneously varied side gate voltages $U_{gL} \propto U_{gR}$ ($y$-axis). As the gate voltage is decreased below $U_{gC} \simeq -1.2$ V lines of conductance maxima form pairs with smaller distance, indicating the deformation of the quantum dot into a double quantum dot (see text). Insets: a SEM micrograph of the top gates with sketches of the approximate potential shapes of the quantum dot or double quantum dot. The third inset shows a sketch of the stability diagram as expected for the case of a double quantum dot. The thick solid lines are guides for the eye.

$G(T) = G_0(T_K'^2/(T^2 + T_K'^2))^s + G_{offset}$ with $T_K' = T_K/\sqrt{2^{1/s} - 1}$ [25]. The low-temperature limit of the Kondo differential conductance $G_0$ is taken as a free parameter, as well as an offset $G_{offset}$ that has been introduced to take into account the effect of the temperature-independent background current described above. For $s = 0.22$ as expected for spin-1/2 Kondo effect [25] we find best agreement between the model and our data at a Kondo temperature of $T_K = 1.9$ K, a limit Kondo conductance $G_0 = 0.41\, e^2/h$ and a conductance offset $G_{offset} = 0.73\, e^2/h$. All nearby areas of enhanced Kondo differential conductance display a similar behaviour with Kondo temperatures in the range of $1.2\text{ K} \lesssim T_K \lesssim 2.0$ K.

In addition, the dependence of the differential conductance $G$ on the source–drain voltage $U_{SD}$ has been measured for different regions of the parameter range in figure 3(a) (data not shown). These measurements are fully consistent with above results. They display a zero-bias conductance anomaly in the high-conductance 'Kondo' regions, that can be suppressed by changing the magnetic field $B_\perp$.

## 4. Deformation into a double quantum dot

The shape of the confinement potential of our quantum dot can be modified by changing the voltages applied to the split gate electrodes. This is a general feature of electrostatically defined structures in a 2DES. A non-parabolic confinement potential is, for example, discussed by the authors of [10]. Here, we demonstrate a controlled deformation of the confinement potential, transforming one local minimum, i.e. a quantum dot, into a double well potential describing a double quantum dot. Such a transition is shown in figure 4, which plots Coulomb blockade oscillations of differential conductance (colour scale) as a function of the centre gate voltage $U_{gC}$ along the $x$-axis. We aim to transform a quantum dot charged by $N = 0, 1, 2, \ldots$ electrons into a peanut-shaped double quantum dot with the same charge (see insets of figure 4). This

is done by creating a high potential ridge between gates $g_X$ and $g_C$, i.e. by making $U_{gC}$ more negative. In order to keep the overall charge of our device constant, both side gate voltages $U_{gL}$ and $U_{gR}$ ($y$-axis) are changed in the opposite direction than $U_{gC}$. For the opposed centre gate $g_X$ we choose $U_{gX} = -0.566$ V, causing a significantly higher potential than in the previous measurements.

For $U_{gC} \gtrsim -1$ V the Coulomb oscillations are to first order quasiperiodic, as can be seen in the upper-right quarter of figure 4. This is expected for a single quantum dot with addition energies large compared to the orbital quantization energies. In contrast, for more negative $U_{gC}$ an onset of a doubly periodic behaviour is observed. That is, along the thick solid horizontal line in the lower-left corner of figure 4 the distance between adjacent conductance maxima oscillates, most clearly visible for $N < 4$. Such a doubly periodic behaviour is expected for a double quantum dot in case of a symmetric double well potential. This is the case along the thick solid line in the inset of figure 4 sketching the double quantum dot's stability diagram. In a simplified picture, if the double quantum dot is charged by an odd number of electrons the charging energy for the next electron is approximately given by the *interdot* Coulomb repulsion of two electrons separated by the tunnel barrier between the adjacent quantum dots. However, for an even number of electrons the charging energy for the next electron corresponds to the larger *intradot* Coulomb repulsion between two electrons confined within the same quantum dot. Therefore, the difference between *interdot* and *intradot* Coulomb repulsion on a double quantum dot causes the observed doubly periodic oscillation.

The asymmetry of the double quantum dot with respect to the potential minima of the double well potential can be controlled by means of the side gate voltages $U_{gL}$ and $U_{gR}$. Coulomb blockade results in a stability diagram characteristic for a double quantum dot as sketched in an inset of figure 4 depending on the side gate voltages [31–33]. Grey lines separate areas of stable charge configurations. The corners where three different stable charge configurations coexist are called triple points of the stability diagram. For a serial double quantum dot with weak interdot tunnel coupling, the charge of both quantum dots can fluctuate only near the triple points and only here is current expected to flow. The bisector of the stability diagram (solid bold line in the inset) defines a symmetry axis, along which the double well potential and, hence, the charge distribution in the double quantum dot is symmetric. In the case of two (one) trapped conduction band electrons we identify our structure as an artificial two-dimensional helium (hydrogen) atom that can be continuously transformed into an (ionized) molecule consisting of two hydrogen atoms.

To prove the presence of a few-electron double quantum dot after performing the described transition, we plot in figure 5 the measured stability diagram of our device. Figure 5(a) shows the linear response dc current through the device ($U_{SD} = 50\,\mu$V) as a function of the side gate voltages $U_{gL}$ and $U_{gR}$. Figure 5(b) displays the QPC transconductance $G_T \equiv \mathrm{d}I_{QPC}/\mathrm{d}U_{gL}$. The areas of stable charge configurations are marked by numerals indicating the number of conduction band electrons in the left/right quantum dot [11, 12]. Both plots clearly feature areas of stable charge configurations separated by either a current maximum (in (a)) or a transconductance minimum (in (b)), respectively. The transconductance measurement confirms the electron numbers obtained from the single quantum dot case, as even for very asymmetric confinement potential no further discharging events towards more negative gate voltages $U_{gL}$ and $U_{gR}$ are observed. In comparison to the grey lines in the inset of figure 4, the edges of the hexagon pattern are here strongly rounded. This indicates a sizable interdot tunnel coupling that cannot be neglected compared to the interdot Coulomb interaction [11, 12]. A large interdot tunnel coupling results in molecular states delocalized within the double quantum dot. This additionally explains the observation of finite current not only on the triple points of the stability diagram, but also along edges of stable charge configurations in figure 5(a). Here the

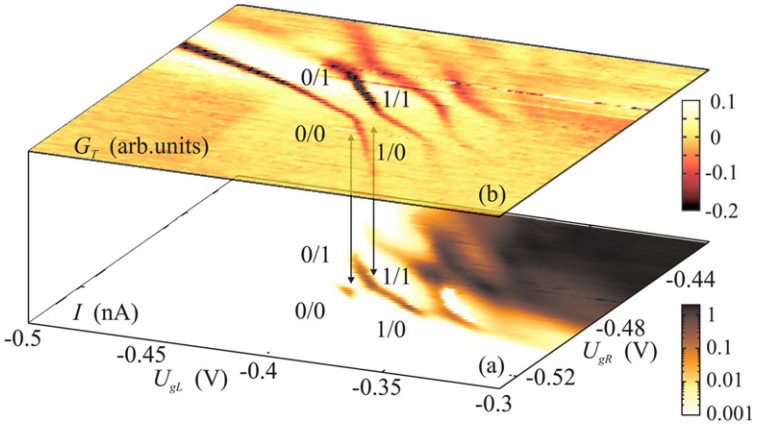


**Figure 5.** (a) The dc current through the double quantum dot, and (b) the transconductance $G_{\mathrm{T}} \equiv \mathrm{d}I_{\mathrm{QPC}}/\mathrm{d}U_{\mathrm{gL}}$ of the nearby QPC used as a double quantum dot charge sensor, with identical axes $U_{\mathrm{gL}}$ and $U_{\mathrm{gR}}$. The additional gate voltages are in both plots chosen as $U_{\mathrm{gC}} = -1.4$ V, $U_{\mathrm{gX}} = -0.566$ V, and $U_{\mathrm{gQPC}} = -0.458$ V.

total charge of the molecule fluctuates, allowing current via a delocalized state. In previous publications the low-energy spectrum of the observed double well potential was analysed and the tunability of the tunnel coupling demonstrated [11, 12].

## 5. Summary

Using a triangular gate geometry, a highly versatile few-electron quantum dot has been defined in the 2DES of a GaAs/AlGaAs heterostructure. The couplings between the quantum dot and its leads can be tuned in a wide range. For weak quantum dot–lead coupling, the shell structure of the states for $1 \lesssim N \lesssim 7$ trapped conduction band electrons is observed. The transport spectrum supports the assumption of a Fock–Darwin-like trapping potential and subsequent filling of spin-degenerate states. For strong quantum dot–lead coupling, a chessboard pattern of regions of enhanced zero bias conductance as a function of a magnetic field perpendicular to the 2DES and the centre gate voltage is observed. The enhanced conductance regions are explained in terms of the Kondo effect, induced by the formation of Landau-like core and ring states in the quantum dot. Finally, for strongly negative centre gate voltages, the quantum dot trapping potential can be distorted at constant charge into a peanut-shaped double quantum dot with strong interdot tunnel coupling.

## Acknowledgments

We would like to thank L Borda and J P Kotthaus for helpful discussions. We acknowledge financial support by the Deutsche Forschungsgemeinschaft via the SFB 631 'Solid state based quantum information processing' and the Bundesministerium für Bildung und Forschung via DIP-H.2.1. A K Hüttel thanks the Stiftung Maximilianeum for support.

## References

[1] Kouwenhoven L P, Marcus C M, McEuen P L, Tarucha S, Westervelt R M and Wingreen N S 1997 *Electron Transport in Quantum Dots* Series E, vol. 145 (*Proceedings of the NATO Advanced Study Institute on Mesoscopic Electron Transport*) (Dordrecht: Kluwer) p 105

[2] Ciorga M, Sachrajda A S, Hawrylak P, Gould C, Zawadzki P, Jullian S, Feng Y and Wasilewski Z 2000 *Phys. Rev.* B **61** 16315
[3] Elzerman J M, Hanson R, Greidanus J S, Willems van Beveren L H, De Franceschi S, Vandersypen L M K, Tarucha S and Kouwenhoven L P 2003 *Phys. Rev.* B **67** 161308
[4] Petta J R, Johnson A C, Marcus C M, Hanson M P and Gossard A C 2004 *Phys. Rev. Lett.* **93** 186802
[5] Pioro-Ladrière M, Abolfath M R, Zawadzki P, Lapointe J, Studenikin S A, Sachrajda A S and Hawrylak P 2005 *Phys. Rev.* B **72** 125307
[6] Loss D and DiVincenzo D P 1998 *Phys. Rev.* A **57** 120
[7] van der Wiel W G, Fujisawa T, Tarucha S and Kouwenhoven L P 2001 *Japan. J. Appl. Phys.* **40** 2100
[8] Field M, Smith C G, Pepper M, Ritchie D A, Frost J E F, Jones G A C and Hasko D G 1993 *Phys. Rev. Lett.* **70** 1311
[9] Sprinzak D, Ji Y, Heiblum M, Mahalu D and Shtrikman H 2002 *Phys. Rev. Lett.* **88** 176805
[10] Kyriakidis J, Pioro-Ladrière M, Ciorga M, Sachrajda A S and Hawrylak P 2002 *Phys. Rev.* B **66** 035320
[11] Hüttel A K, Ludwig S, Lorenz H, Eberl K and Kotthaus J P 2005 *Phys. Rev.* B **72** 081310(R)
[12] Hüttel A K, Ludwig S, Lorenz H, Eberl K and Kotthaus J P 2006 *Physica* E **34** 488
[13] Schröer D M, Hüttel A K, Eberl K, Ludwig S, Kiselev M N and Altshuler B L 2006 *Phys. Rev.* B **74** 233301
[14] Fock V 1928 *Z. Phys.* **47** 446
[15] Darwin C G 1930 *Proc. Camb. Phil. Soc.* **27** 86
[16] Hüttel A K, Ludwig S, Eberl K and Kotthaus J P 2006 *Physica* E **35** 278
[17] Ashoori R C, Stormer H L, Weiner J S, Pfeiffer L N, Baldwin K W and West K W 1993 *Phys. Rev. Lett.* **71** 613
[18] Tarucha S, Austing D G, Honda T, van der Hage R J and Kouwenhoven L P 1996 *Phys. Rev. Lett.* **77** 3613
[19] Fuhrer A, Lüscher S, Ihn T, Heinzel T, Ensslin K, Wegscheider W and Bichler M 2001 *Nature* **413** 822
[20] Lüscher S, Heinzel T, Ensslin K, Wegscheider W and Bichler M 2001 *Phys. Rev. Lett.* **86** 2118
[21] Kouwenhoven L P, Austing D G and Tarucha S 2001 *Rep. Prog. Phys.* **64** 701
[22] Pioro-Ladrière M, Usher A, Sachrajda A S, Lapointe J, Gupta J, Wasilewski Z, Studenikin S and Elliott M 2006 *Phys. Rev.* B **73** 075309
[23] Kondo J 1964 *Prog. Theor. Phys. (Kyoto)* **32** 37
[24] Goldhaber-Gordon D, Shtrikman H, Mahalu D, Abusch-Magder D, Meirav U and Kastner M A 1998 *Nature* **391** 156
[25] Goldhaber-Gordon D, Göres J, Kastner M A, Shtrikman H, Mahalu D and Meirav U 1998 *Phys. Rev. Lett.* **81** 5225
[26] Schmid J, Weis J, Eberl K and von Klitzing K 2000 *Phys. Rev. Lett.* **84** 5824
[27] McEuen P L, Foxman E B, Kinaret J, Meirav U, Kastner M A, Wingreen N S and Wind S J 1992 *Phys. Rev.* B **45** 11419
[28] Keller M, Wilhelm U, Schmid J, Weis J, von Klitzing K and Eberl K 2001 *Phys. Rev.* B **64** 033302
[29] van der Vaart N C, de Ruyter van Steveninck M P, Kouwenhoven L P, Johnson A T, Nazarov Y V, Harmans C J P M and Foxon C T 1994 *Phys. Rev. Lett.* **73** 320
[30] Stopa M, van der Wiel W G, De Franceschi S, Tarucha S and Kouwenhoven L P 2003 *Phys. Rev. Lett.* **91** 046601
[31] Hofmann F, Heinzel T, Wharam D A, Kotthaus J P, Böhm G, Klein W, Tränkle G and Weimann G 1995 *Phys. Rev.* B **51** 13872
[32] Blick R H, Pfannkuche D, Haug R J, von Klitzing K and Eberl K 1998 *Phys. Rev. Lett.* **80** 4032
[33] van der Wiel W G, Franceschi S D, Elzerman J M, Fujisawa T, Tarucha S and Kouwenhoven L P 2003 *Rev. Mod. Phys.* **75** 1